Author Manuscript

Published in final edited form as:

Experimental Mechanics (2020) 60:119 – 128

Doi: 10.1007/s11340-019-00545-9

Title:

Experimental Evaluation of Vertebral Strain in Lumbar Total Disc Replacement

*A.Semitela[1], F. Fonseca[2], A. Completo[1]**

[1] Department of Mechanical Engineering, University of Aveiro, Portugal

[2] Department of Orthopaedics, Coimbra University Hospital, Portugal

Corresponding Author: *António Completo. Email: completo@ua.pt

Abstract

Background mainly in the United States, because the insurance companies have refused to reimburse surgeons for fear of delayed complications, revisions and unknown secondary costs. Typical long-term vertebrae-implant related structural complications include subsidence, migration, implant displacement, endplate fracture, wear and loosening. Intervertebral disc implant size, shape, position, endplate removal and compressive strength of trabecular bone further affect the risk of implant subsidence and loosening. The aim of the present study is to understand the combined effects of the different depth positioning of the ProDisc-L implant and endplate removal during surgery on the vertebral bone strain behaviour. Manufactured synthetic spinal L3-L4 segments were used to experimentally predict vertebrae cortex strain behaviour for different depth implant positioning and endplate thickness removal. In addition, validated finite element models were developed to assess the structural behaviour of cancellous-bone. Measured cortex strains showed significant differences relative to the intact vertebra for the most extreme depth implant positioning. The endplate thickness reduction tends to decrease significantly compressive cortex strains for all strain gauges. A two- to three-fold cancellous-bone strain increase occurs when more than 50% of the endplate thickness is removed, independently of the depth implant position. It is concluded that the implanted strain distribution that better fits intact vertebra strain behaviour is achieved when the depth centred implant position is combined with a partial endplate thickness removal.

Keywords: experimental strains; strain gauge; lumbar total disc replacement; strain-shielding; ProDisc-L; finite element model.

Introduction

Total disk replacement (TDR) has met considerable resistance from the medical community, mainly in the United States, because insurers have refused to reimburse surgeons for TDRs due to concerns with delayed complications, revisions, and unknown secondary costs [1-2]. Although some short-term clinical follow-up studies indicate satisfactory outcomes, there is a lack of long-term clinical data proving the efficacy of the TDR [3-5]. Typical long-term vertebrae-implant related structural complications include subsidence, migration, implant displacement, endplate fracture, wear and loosening [6]. Intervertebral disc implant size, shape, position, endplate removal and compressive strength of trabecular bone affect the risk of implant subsidence and loosening [7-10]. The proportion of current TDR patients who will ultimately develop subsidence and loosening will increase, as the predominantly younger TDR population ages and experiences progressive bone loss and osteoporosis [11]. Parameters, such as implant positioning combined with cortical endplate preparation (removal), are related to the patient's anatomy and condition, as well as, on the level of experience of the surgeon. These vertebral structural parameters are more critical when constrained-keeled implants are used, as the case of ProDisc-L, since these devices seem to be less forgiving and need particular anatomic placement, and the keel affects the mechanical integrity of the endplate [9,12]. To the authors' knowledge, very little experimental work has been published about the strain/stress behaviour of the implanted lumbar vertebrae. The aim of the present study is to understand the combined effects of different depth positioning of the ProDisc-L implant and endplate removal (thickness) on the vertebral bone strain behaviour. Ideally, vertebral bone strain values should be low enough to avoid exceeding the bone fatigue levels, which are related to risk of implant subsidence and vertebral facture, but also, must not be below bone-remodelling inductive levels, which lead to bone atrophy, ultimately resulting in implant loosening in the long term.

Experimental procedure

Five simplified L3-L4 synthetic lumbar spine segments had to be manufactured because they were not commercially available. Each segment includes a L3 and L4 synthetic lumbar vertebra (models 3429-3-2 and 3429-4-2, from Pacific Research Labs, WA, USA) with a solid foam cancellous core (solid rigid polyurethane foam) and a simulated cortical bone (short fiber filled epoxy) and three mimetic synthetic intervertebral discs L2/3, L3/4 and L4/5 (Figure 1). The synthetic intervertebral discs were manufactured in order to mimetic the functional structure of the natural disc, with a solid annulus composed by concentric silicone rubber layers and a nucleus filled with an incompressible gelatin-hydrogel (Figure 1). The dimensions of each synthetic disc were determined from morphological studies of human intervertebral disc [13-14], which are presented in table 1. The number of silicone rubber layers (1mm/layer) on annulus was defined based on experiments in order to approximate the dynamic compressive axial stiffness of the human interval disc with values ranging between 1189N/mm and 2480N/mm [15-16] (Table 1). The three discs were rigidly fixed to the L3 and L4 vertebrae endplates as well as to the upper and lower compression plates with epoxy resin (Figure 1). Ten triaxial rosette strain gauges (KFG-1-120-D17-11L3M2S, Kyowa, Japan) were glued to the anterior (Au, Am, Al), anterolateral (ALu, ALm, ALl), posterolateral (PLu, PLm, PLl) and posterior (Pu) sides of the L4 vertebral body (Figure 1). All strain gauges were connected to a data acquisition system PXI-1050 (National Instruments, USA). Each intact L3-L4 spinal segment was subjected to an axial cyclic (1Hz) compressive load of 1200N, based on the ASTM F2423-11 standard for testing of lumbar IVD prosthesis [17], applied through an electromechanical load device on the upper compression plate (Figure 1). To provide a better control of the load delivered to the vertebral body, there was no inter-contact of the posterior vertebrae facets joints. The implanted models were constructed from the intact models (the same vertebrae were used to test both the intact

and the implanted models), in order to test three different depth implant positioning; anterior, centered and posterior which were combined with three L4 vertebra upper endplate thicknesses (Figure 2). The anterior and posterior implant positions correspond to the maximum anterior and posterior endplate borders fit (depth range ≈7mm). The ProDisc-L (DePuy Synthes, Raynham, MA, USA) prosthesis (size M, 6º) implantation procedure was done by an experienced surgeon, according to the protocol described for this prosthesis [18] with the partial removal of the L3/4 disk (Figure 2). The test procedure for each implanted spine specimen begins with the intact L4 vertebra endplate (≈0,5mm thickness, measured by CT-scan), then the upper vertebra endplate thickness was reduced by milling to ≈0,25mm (half of intact endplate thickness) and finally the vertebral endplate is completely removed (≈0mm thickness); the three depth implant positioning were tested for each one endplate thickness. The strain gauge Au (anterior upper) is removed due to the implantation procedure (Figure 3). Each implanted L3-L4 spine segment was subjected to the same load condition of the intact spine (Figure 3). In order to evaluate the L4 vertebra cortex strain changes between intact and the nine different implanted cases, as well as establish the correlations with FE models the maximum-ε1 and minimum-ε2 principal strains within the plane of the gauge at the fifty load cycle were calculated and averaged, and the standard deviations determined. Normal distribution of all data was evaluated through an exploratory data analysis. A two-way ANOVA was conducted to evaluate the effect of each of the two independent variables (endplate thicknesses and depth implant positioning) and their interaction. Additionally, paired t-tests were performed to assess the statistical significant difference of the mean principal strains between intact and implanted state. The spine L3-L4 segment displacement was also measured.

Finite element analysis

Finite element (FE) models of intact and implanted L3-L4 spine segments were made from CT-scans of the experimental models, which were then converted to 3D models with an image processing software (ScanIP, Simpleware Ltd. Exeter, UK). The implant geometries were created with the CAD modeling package Catia V5 (Dassault-Systèmes, France) after 3D digitalization. The number of elements (Table 2) was chosen based on convergence tests, of the spine segment axial displacement and the minimum principal strains at two locations. The convergence rate of the displacements was less than 1% and less than 3% for the minimum principal strains when nearly 190,000 elements were used. The disc nucleus was modelled as incompressible fluid - filled cavity with a density of 1.27 g/cm^-3. Tie constraints were used between vertebrae and respective contacting surface of the disc (annulus and nucleus). All implant-vertebrae interfaces were considered to be in contact, with a friction coefficient of 0.8 to mimic the effect of the small teeth and prosthesis surface asperities [19-20]. The metal-on-polyethylene contact was modelled with a friction coefficient of 0.083 [21]. All contacts were modelled with a surface-to-surface contact algorithm and with the augmented Lagrange formulation method. The material properties used were those described by the manufacturer (Table 2) and were assumed to be homogeneous, isotropic and linear elastic. All simulations were conducted using the commercial software Abaqus v. 6.14 (Dassault Systèmes Simulia Corp.). Nonlinear geometry effects were accounted for in all simulations. Applied load was identical to the experimental models. Regression analyses between the principal strains predicted by the FE models and experimentally measured strains were performed. The overall absolute difference between numerical and experimental cortex strains, the root-mean-square-error was calculated and expressed as a percentage of the peak values of the measured principal strains (RMSE %). The spine segment displacement for each model was compared with the experimental. Principal minimum cancellous-bone strains were analysed/compared between intact and implanted models.

Results

Figure 3 shows the means and standard deviations of the cortex principal strains for the three implant depth positioning's tested combined with a L4 vertebra endplate thickness of 0.5mm (Fig. 3a), 0.25mm (Fig. 3b) and 0mm (Fig. 3c). The average standard deviation of the principal cortex strains was less than 11%. Analogous cortex strain behaviour between strain gauges was observed for the three endplates thicknesses tested (Fig 3a, Fig.3b and Fig. 3c).

To evaluate the effect of each of the two independent variables (endplate-thickness and depth-implant-positioning) and their interaction, the two-way ANOVA analysis was done and the results are presented in Table 3. These results confirmed that there are significant differences ($p<0.05$) between the minimum principal cortex strain ($\varepsilon 2$) results for the different endplate thicknesses for all strain gauges at exception of the AL_upper strain gauge. The maximum principal strain ($\varepsilon 1$) results differ significantly ($p<0.05$) between the different endplate thicknesses on four strain gauges the A_midlle, AL_lower, AL_upper and P_upper. Regarding the different depth implant positioning there are significant differences ($p<0.05$) between the minimum principal cortex strain ($\varepsilon 2$) results on all strain gauges. The maximum principal strains ($\varepsilon 1$) results differ significantly ($p<0.05$) between different depth implant positioning on all strain gauges at the exception of two strain gauges, the PL_middle and PL_lower. There are no significant differences ($p>0.05$) on the minimum principal strains ($\varepsilon 2$) results in the interaction between endplate thicknesses and depth implant positioning on three strain gauges the A_lower, AL_upper and AL_lower. Concerning the maximum principal strains ($\varepsilon 1$) results, no significant difference ($p>0.05$) in the interaction between endplate thicknesses and depth implant positioning were found on five strain gauges the A_middle, AL_middle, AL_lower, PL_upper and PL_lower.

The greatest nominal cortex principal strain differences relatively to the intact condition occur for the most extreme depth implant positioning (Anterior and Posterior) at Am, ALu, ALm, PLu and Pu strain gauges positions (Figure 3). The endplate thickness reduction tends to decrease minimum principal strains for all strain gauges and increase maximum principal strains in anterior (Am) and posterior (Pu) strain gauges relatively to the intact segment (Figure 3). Significant principal cortex strain differences ($p<0.05$) between intact and all implanted cases are presented in Table 4. The endplate thickness reduction increases the number of strain gauges (for all depth implant positioning) with significant ($p<0.05$) minimum principal strain differences between intact and implanted cases (Table 4).

Figure 4 presents the linear regressions curves for intact and the three depth implanted positions with a 0.5mm (Fig 4a), 0.25mm (Fig.4b) and 0mm (Fig. 4c) endplate thickness. The linear regression correlation values (R^2) between numerical and experimental cortex strains for the ten analysed cases ranged between 0.91 and 0.96 with slopes ranged between 0.97 and 1.05 (Figure 4). The measured displacement of the intact segment was 1.77±0.18mm and 1.16±0.12mm in implanted cases. The FE displacement of the intact model was 1.61mm while implanted segments ranged between 1.07 and 1.04mm, which represents less than 10% relatively to experimental ones. The overall absolute difference between numerical and experimental cortex strains (RMSE %) comprising all models was 12%. Figure 5 shows the minimum principal strains patterns in L4 vertebra cancellous-bone obtained in the FE analysis. The highest cancellous-bone strain differences were inferior to 25% between the three depth implant positions, for an identical endplate thickness. The endplate thickness reduction increases nominal strain values relatively to the intact model, a two-three fold cancellous-bone strain increase occurs when the endplate is totally removed (Figure 5).

Discussion

The aim of the present work was to investigate in-vitro implant–vertebra load transfer mechanisms, particularly the effect of depth implant positioning combined with the cortical endplate removal on the vertebral bone strain behaviour. The standard deviations of the measured vertebra cortex strains were within the range of those found in the literature which used other synthetic bones [22-23]. The two-way ANOVA analysis indicates that there is a significant effect on minimum and maximum principal cortex strain results between the different depth implant positioning, for most of the strain gauges. Concerning the different endplate thickness factor, there is a significant effect on the minimum principal strains results for the majority of strain gauges, while for the maximum principal strains results this factor is not significant for most of the strain gauges. Furthermore, there is a combined effect on the minimum principal cortex strains results in the interaction between endplate thicknesses and depth implant positioning for most of strain gauges positions, while for the maximum principal strains results this interaction is absent in the majority of strain gauges. These experimental cortex strain results, in particular the minimum principal strains, show that the implanted vertebral body is susceptible to the different combinations of depth implant positioning and endplate thickness.

The depth centred implant position models were those that presented the closest behaviour to that of the intact vertebra cortex strain, while the posterior depth implant positioning caused an extreme strain increase (four-fold) at the posterior vertebral surface which reveals some potential risk of fatigue fracture resulting from bone microdamage due to excessive cyclic loading [24-25]. The implanted cases with the intact endplate thickness ($t \approx 0.5$mm) were those that followed most closely the intact vertebra cortex strain behaviour independently of the depth implant position. Significant minimum principal cortex strain reduction occurs when more than 50% of the intact endplate

thickness was removed; however, the nominal cortex strain reduction (<150μstrain) does not appear to induce an important cortex structural risk at long-term [26].

The developed FE models present linear regressions and RMSE values in the range of other experimental-numerical studies performed using synthetic bones [27, 28], which reveal good agreement between FE and measured cortex strains. Intact vertebra cancellous-bone strain behaviour revealed that the highest nominal minimum principal strains take place in the vertebral centrum region, which is in agreement with the major load-bearing pathway in axil compression with a nondegenerate disc [29-30]. The peak cancellous-bone strain differences between the three depth implanted positions, for identical endplate thickness, were small. The depth centred implant position was the one that better followed the intact vertebra cancellous-bone strain behaviour. The intact endplate thickness models presented a cancellous-bone strain reduction, under the implant footplate, relatively to the intact vertebra, for all depth implant positions. It is known that in situations where bone loads are reduced or eliminated, bone mass is reabsorbed [31-32], which can represent a potential structural risk at long-term. However, the intermediate endplate thickness (0.25mm) fits the intact vertebra strain behaviour at the central body region without signs of strain-shielding effect. A substantial cancellous-bone strain increase (>100%) occurs when the endplate was completely removed (0mm) for all depth implant positions. The failure process of cancellous-bone can be due to overload, normally through a fatigue mode, and it may occur if compressive strains are increased by 50% to 100% due to prosthesis implantation [33-34], which is the present case.

Few experimental studies analysed lumbar vertebra cortex strains [35-37], all of them on the intact cadaveric vertebrae; however, the different load magnitude, fixture setup and vertebral bone condition do not allow a direct cortex strain comparison. Intact cortex

strains, at equivalent vertebral body regions, between 400 and 2500 microstrain were found for a 1470 N axial compressive load [36] and 100 to 700 microstrain for a compressive load of 490N [37], such cortex strains are in the range of the present study, for the intact case, if the applied load is scaled.

As in all experimental-numerical studies, the present study had some shortcomings one such limitation is concerned with the use of synthetic bones and synthetic intervertebral discs. The mechanical changes on the gelatin-hydrogel intervertebral disc after testing were not evaluated in this study, which can be considered a limitation. Nevertheless, each gelatin-hydrogel intervertebral disc was only loaded one time in each intact model. Furthermore, using different synthetic vertebral segments for each of the experimental groups would mitigate the effect of previous loading on the vertebrae strain measured. The advantage of using artificial bones and intervertebral disc is that specimen geometry and material is near constant, which optimizes the reproducibility of results obtained in experimental tests. Experimental load configuration was simplified with the vertebral body only loaded through its adjacent discs. However, the applied load is representative of major load acting upon the vertebral body and implant; on the erect standing posture, when the disc is normal, the neural arch resists only 8% of the applied compressive force, and the remainder is distributed on the vertebral body [38]. Furthermore, due to the comparative nature of the study, it is concluded that the observed strain results are representative of major strain differences between intact and the different implanted states at the same strain measurement location.

The main finding of the present study is that the depth implant positioning combined with the endplate thickness changes considerably the magnitude of vertebral bone strains relative to the intact state. Independently of implant depth position, significant reduction of endplate thickness yields an important structural risk, which can be associated with the

fatigue failure process of cancellous-bone due to overload. However, implanted cases with no endplate removal, the unloaded bone region under the implant footplate can be subjected to localized bone mass resorption at long-term. The strain distribution that better fits intact vertebra strain behaviour is achieved by the depth centered implant position combined with a partial endplate thickness removal.

Acknowledgements

The authors acknowledge the financial support through project POCI-01-0145-FEDER-028424- PTDC EME-SIS 28424 2017, which was funded by the Operational Program for Competiveness and Internationalization (COMPETE 2020) in its component FEDER and by Science and Technology Foundation (FCT) through the OE budget. The authors also acknowledge FCT grant UID/EMS/00481/2019–FCT and the infrastructures support CENTRO-01-0145-FEDER-022083-Centro Portugal Regional Operational Programme (Centro2020).

REFERENCES

1. Sandhu F, Blumenthal S, Grunch B, Kimball B, Ferko N, Hollmann S (2017) Barriers to and Budget Impact of Lumbar Total Disc Replacement Utilization. Spine. 42: Suppl 24:S112-S114.

2. Hart RA, DePasse JM, Daniels AH (2017) Failure to Launch: What the Rejection of Lumbar Total Disk Replacement Tells us About American Spine Surgery. Clin Spine Surg. 30:E759-E764.

3. Siepe CJ, Heider F, Wiechert K, Hitzl W, Ishak B, Mayer MH (2014) Mid- to long-term results of total lumbar disc replacement: a prospective analysis with 5- to 10-year follow-up. Spine J 14:1417-1431.

4. Garcia R Jr, Yue JJ, Blumenthal S, Coric D, Patel VV, Leary SP, Dinh DH, Buttermann GR, Deutsch H, Girardi F, Billys J, Miller LE (2015) Lumbar Total Disc Replacement for Discogenic Low Back Pain: Two-year Outcomes of the activL Multicenter Randomized Controlled IDE Clinical Trial. Spine. 40:1873-1881.

5. Salzmann SN, Plais N, Shue J, Girardi FP (2017) Lumbar disc replacement surgery-successes and obstacles to widespread adoption. Curr Rev Musculoskelet Med. 10:153-159.

6. Formica M, Divano S, Cavagnaro L, Basso M, Zanirato A, Formica C, Felli L (2017) Lumbar total disc arthroplasty: outdated surgery or here to stay procedure? A systematic review of current literature. J Orthop Traumatol. 18 :197-215.

7. Lee CK. (2007) Osteopenia and total disc prosthesis subsidence: inclusion/exclusion criteria for total disc replacement. SAS J. 1: 82-84

8. Auerbach JD, Ballester CM, Hammond F, Carine ET, Balderston RA, Elliott DM (2010) The effect of implant size and device keel on vertebral compression properties in lumbar total disc replacement. Spine J. 10: 333-340.

9. Oxland TR, Grant JP, Dvorak MF, et al. (2003) Effects of endplate removal on the structural properties of the lower lumbar vertebral bodies. Spine 28:771–777.

10. Zigler, J, Garcia R.. (2015) ISASS Policy Statement - Lumbar Artificial Disc. Int J Spine Surg. 9, 7.

11. Osterhoff G, Morgan EF, Shefelbine, SJ, Karim L, McNamara LM, Augat P (2016) Bone mechanical properties and changes with osteoporosis. Injury. 47, S11-S20.

12. Auerbach, JD, Ballester CM, Hammond F, Carine,ET, Balderston RA, Elliott DM (2010) The effect of implant size and device keel on vertebral compression properties in lumbar total disc replacement. Spine J. 10, 333-340.

13. Zhou SH, McCarthy ID, McGregor AH, Coombs RR, Hughes SP (2000) Geometrical dimensions of the lower lumbar vertebrae--analysis of data from digitised CT images. Eur Spine J. 9:242-248.

14. Saraste H, Brostrom LA, Aparisi T, Axdorph G (1985) Radiographic measurement of the lumbar spine – a clinical and experimental study on man. Spine 10:236–241.

15. Kemper AR, McNally C, Duma SM (2007) The influence of strain rate on the compressive stiffness properties of human lumbar intervertebral discs. Biomed Sci Instrum. 43: 176-181.

16. Smeathers JE1, Joanes DN (1988) Dynamic compressive properties of human lumbar intervertebral joints: a comparison between fresh and thawed specimens. J Biomech. 21: 425-433.

17. ASTM F2423-11(2016), Standard Guide for Functional, Kinematic, and Wear Assessment of Total Disc Prostheses, ASTM International, West Conshohocken, PA.

18. Prodisc-L. Modular Intervertebral Disc Prosthesis for Stabilizing the Lumbar Spine and Restoring the Physiological Range of Motion – Surgical Technique (2017) DePuy Synthes Spine, a division of Synthes GmbH..

19. Completo A, Nascimento A, Ramos A, Simões J. (2015) Failure analysis of C-5 after total disc replacement with ProDisc-C at 1 and 2 levels and in combination with a fusion cage: finite-element and biomechanical models. J Neurosurg Spine. 22: 639-646.

20. Polikeit A, Ferguson SJ, Nolte LP, Orr TE (2003) Factors influencing stresses in the lumbar spine after the insertion of intervertebral cages: finite element analysis. Eur Spine J. 12: 413–420..

21. Goreham-Voss CM, Hyde PJ, Hall RM, Fisher J, Brown TD (2010) Cross-shear implementation in sliding-distance-coupled finite element analysis of wear in metal-on-polyethylene total joint arthroplasty: intervertebral total disc replacement as an illustrative application. J Biomech 43:1674–1681.

22. Completo A, Simões J, Fonseca F (2008) Experimental Evaluation of Strain Shielding in Distal Femur in Revision TKA. Experimental Mechanics 48: 817-824.

23 Completo A, Fonseca F, Simões JA, Ramos A, Relvas C (2012) A new press-fit stem concept to reduce the risk of end-of-stem pain at revision TKA: a pre-clinical study. Knee 19: 537-542.

24. Pentecost R, Murray R, Brindley H. Fatigue (1964) Insufficiency, and Pathological Fractures. JAMA. 187: 1001-1004.

25. Lambers F, Bouman A, Rimnac C, Hernandez C (2013) Microdamage caused by fatigue loading in human cancellous bone: relationship to reductions in bone biomechanical performance. PLoS One. 8: e83662.

26. Frost H (2003) Bone's mechanostat: a 2003 update. Anat Rec A Discov Mol Cell Evol Biol. 275: 1081-1101.

27. Heiner A. (2008) Structural properties of fourth-generation composite femurs and tibias. J. Biomech. 41: 3282–3284.

28. Completo A, Duarte R, Fonseca F, Simões JA, Ramos A, Relvas C (2013) Biomechanical evaluation of different reconstructive techniques of proximal tibia in revision total knee arthroplasty: An in-vitro and finite element analysis. Clin Biomech. 28:291-298.

29. Eswaran SK, Gupta A, Adams MF, Keaveny TM. (2006) Cortical and trabecular load sharing in the human vertebral body. J Bone Miner Res. 21:307-14.

30. Ferguson SJ, Steffen T. Biomechanics of the aging spine. (2003) Eur Spine J. 12 Suppl 2:S97-S103.

31. Kerner J, Huiskes R, van Lenthe GH, Weinans H, van Rietbergen B, Engh CA, Amis AA. (1999) Correlation between pre-operative periprosthetic bone density and post-operative bone loss in THA can be explained by strain-adaptive remodelling. J Biomech. 32 :695-703.

32. Gross T, Rubin C. (1995) Uniformity of resorptive bone loss induced by disuse. J. Orthop. Res. 13: 708-714.

33. Taylor M. Tanner K. (1997) Fatigue failure of cancellous bone: a possible cause of implant migration and loosening. J-Bone-Joint-Surg Br. 79: 181-182.

34. Choi K, Goldstein SA. (1992) A comparison of the fatigue behavior of human trabecular and cortical bone tissue. J Biomech. 25:1371-1381.

35. Hongo M, Abe E, Shimada Y, Murai H, Ishikawa N, Sato K. (1999) Surface strain distribution on thoracic and lumbar vertebrae under axial compression. The role in burst fractures. Spine. 24 :1197-1202.

36. Shah JS, Hampson WG, Jayson MI. (1978) The distribution of surface strain in the cadaveric lumbar spine. J Bone Joint Surg Br. 60: 246-51.

37. Cristofolini L, Brandolini N, Danesi V, Juszczyk MM, Erani P, Viceconti M. (2013) Strain distribution in the lumbar vertebrae under different loading configurations. Spine J. 13: 1281-1292.

38. Pollintine P, Dolan P, Tobias JH, Adams MA. (2004) Intervertebral disc degeneration can lead to "stress-shielding" of the anterior vertebral body: a cause of osteoporotic vertebral fracture? Spine. 29: 774-782.

List of figures

FIGURES:

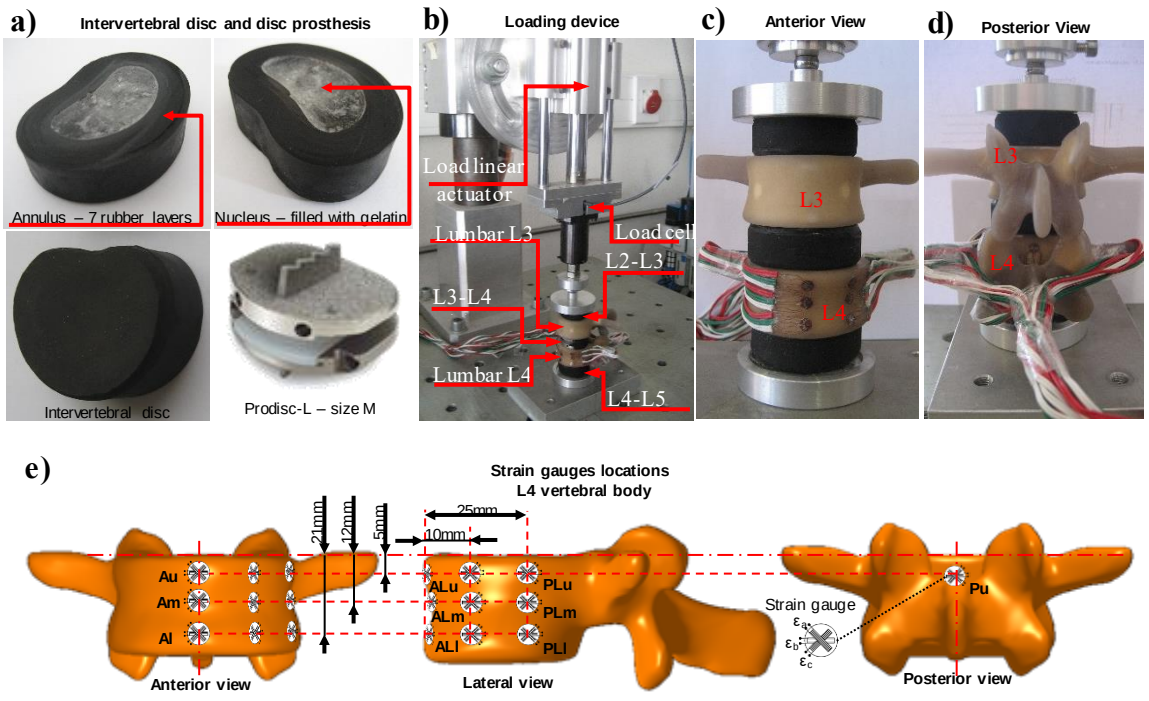

Figure 1

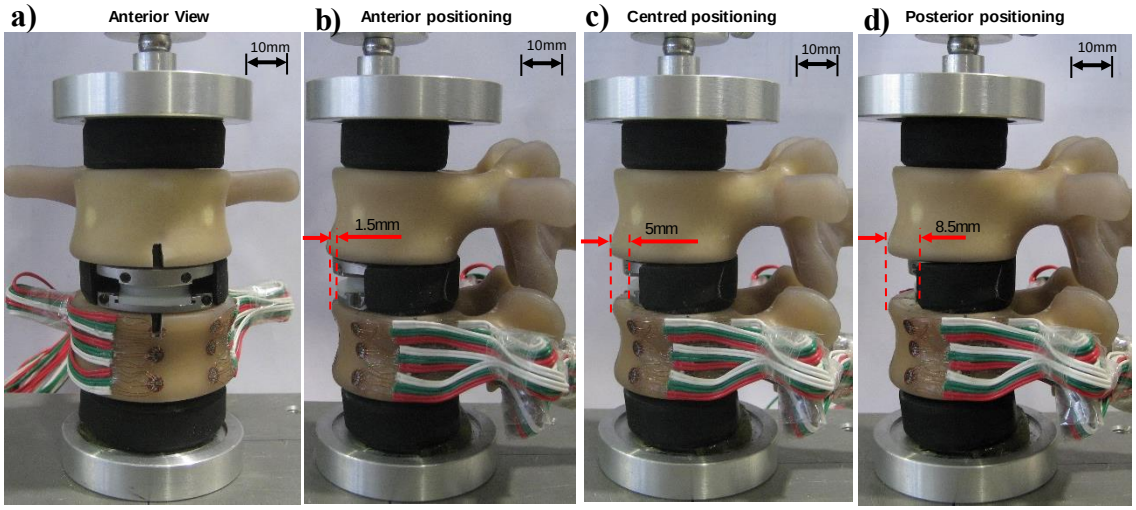

Figure 2

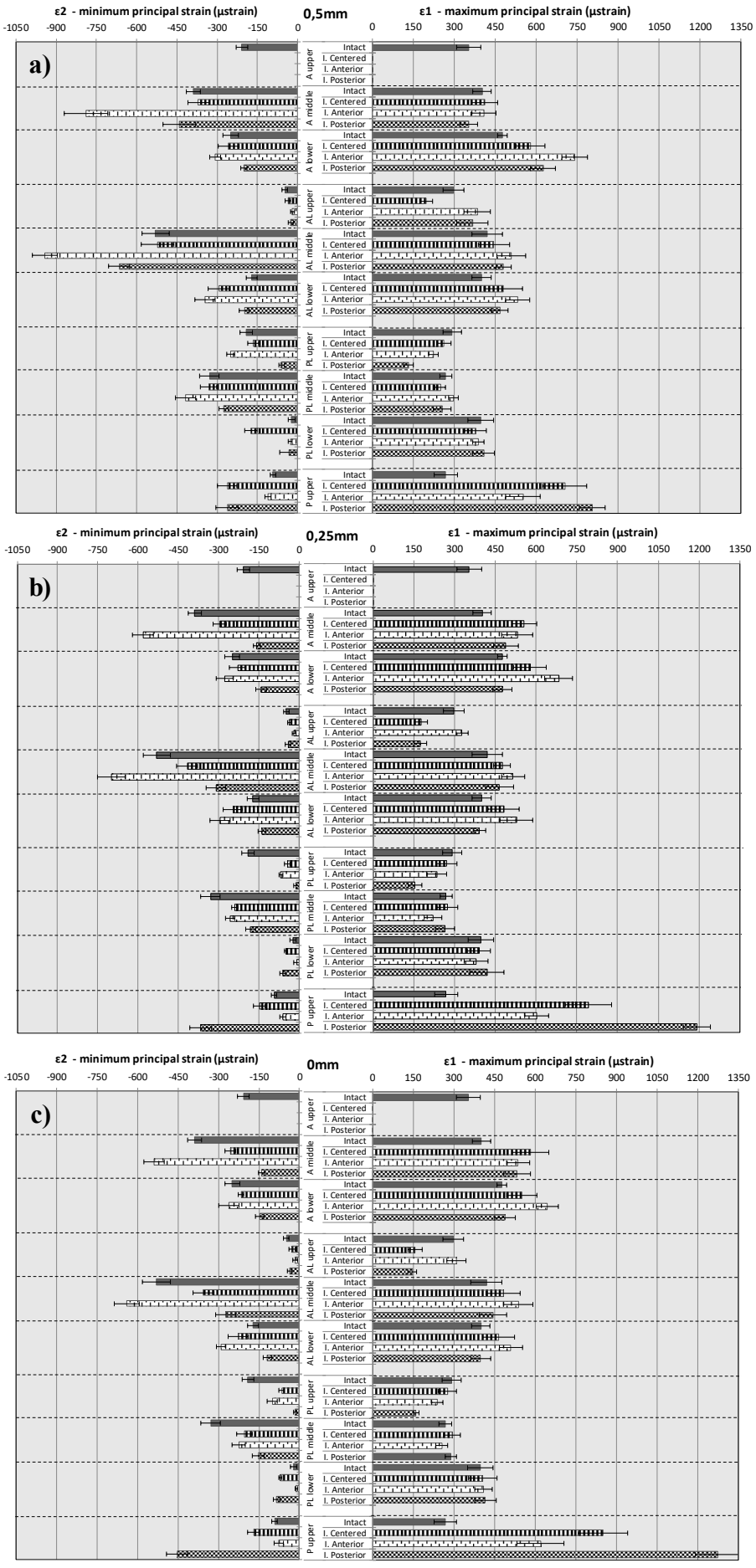
a)
0,5mm
ε2 - minimum principal strain (µstrain)
ε1 - maximum principal strain (µstrain)
-1050 -900 -750 -600 -450 -300 -150 0
0 150 300 450 600 750 900 1050 1200 1350
A upper
A middle
A lower
AL upper
AL middle
AL lower
PL upper
PL middle
PL lower
P upper
Intact
I. Centered
I. Anterior
I. Posterior
b)
0,25mm
ε2 - minimum principal strain (µstrain)
ε1 - maximum principal strain (µstrain)
-1050 -900 -750 -600 -450 -300 -150 0
0 150 300 450 600 750 900 1050 1200 1350
A upper
A middle
A lower
AL upper
AL middle
AL lower
PL upper
PL middle
PL lower
P upper
Intact
I. Centered
I. Anterior
I. Posterior
c)
0mm
ε2 - minimum principal strain (µstrain)
ε1 - maximum principal strain (µstrain)
-1050 -900 -750 -600 -450 -300 -150 0
0 150 300 450 600 750 900 1050 1200 1350
A upper
A middle
A lower
AL upper
AL middle
AL lower
PL upper
PL middle
PL lower
P upper
Intact
I. Centered
I. Anterior
I. Posterior

Figure 3

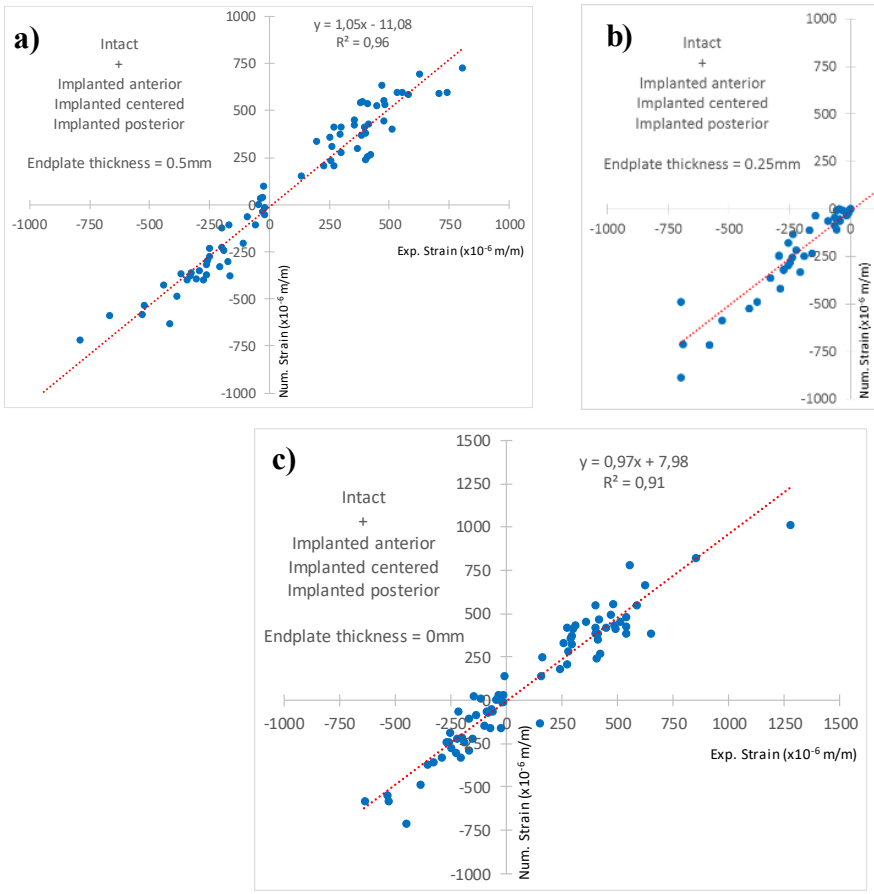
a)
Intact
+
Implanted anterior
Implanted centered
Implanted posterior
Endplate thickness = 0.5mm
y = 1,05x - 11,08
R² = 0,96
Exp. Strain (x10⁻⁶ m/m)
Num. Strain (x10⁻⁶ m/m)
b)
Intact
+
Implanted anterior
Implanted centered
Implanted posterior
Endplate thickness = 0.25mm
y = 0.99x - 6.21
R² = 0.93
Exp. Strain (x10⁻⁶ m/m)
Num. Strain (x10⁻⁶ m/m)
c)
Intact
+
Implanted anterior
Implanted centered
Implanted posterior
Endplate thickness = 0mm
y = 0,97x + 7,98
R² = 0,91
Exp. Strain (x10⁻⁶ m/m)
Num. Strain (x10⁻⁶ m/m)

Figure 4

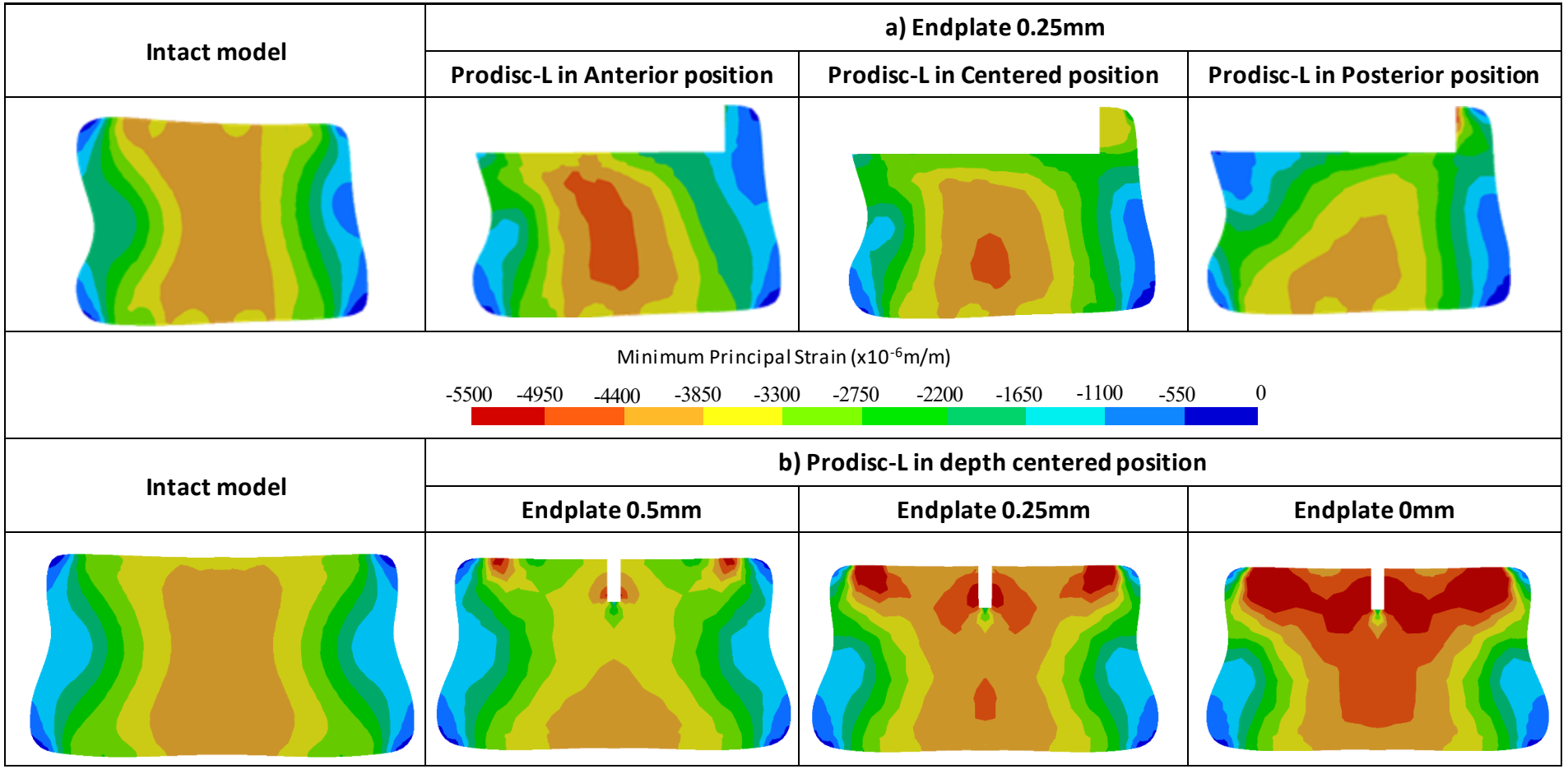
Intact model
a) Endplate 0.25mm
Prodisc-L in Anterior position
Prodisc-L in Centered position
Prodisc-L in Posterior position
Minimum Principal Strain (x10-6m/m)
-5500 -4950 -4400 -3850 -3300 -2750 -2200 -1650 -1100 -550 0
Intact model
b) Prodisc-L in depth centered position
Endplate 0.5mm
Endplate 0.25mm
Endplate 0mm

Figure 5

Table 1 – Mean intervertebral disk dimensions and axial dynamic stiffness.

Intervertebral disc	Height (mm)	Depth (mm)	Width (mm)	Annulus number of silicone rubber layers	Dynamic stiffness at 1Hz (N/mm)
L2/3	11.5	35	48	6	1980±120
L3/4	12	37	54	7	2084±128
L4/5	12	38	54	7	2105±135

Table 2 - Material properties and FE mesh characteristics.

Component	Material	Young modulus (MPa)	Poisson's ratio	Element type	Number of elements	
					Intact	Implanted
Vertebral cortical bone	short fiber filled epoxy	16,000	0.26	C3D10	195,179	205,732
Vertebral cancellous bone	solid rigid polyurethane foam (ρ=0.16g/cm^{-}3)	58	0.3	C3D10		
Disc annulus	silicone rubber	5	0.47	C3D20		
Disc nucleus	hydrogel	incompressible fluid (ρ=1.27 g/cm^{-}3)		SFM3D4		
ProDisc-L Endplates	CrCoMo	21,000	0.3	C3D10		
ProDisc-L Inlay core	UHMWPE	2500	0.45	C3D10		
Compression plates	aluminum	70,000	0.3	C3D10		

Table 3 – P-values from two-away ANOVA to test the effect of each of the two independent variables, endplate thickness and depth positioning, and their interaction.

		Principal strain	
Strain gauge	**Source of Variation**	**ε1 - maximum**	**ε2 - minimum**
A upper		-	-
A middle	Endplate thickness	p<0.05	p<0.05
	Depth implant positioning	p<0.05	p<0.05
	Interaction	0,78	p<0.05
A lower	Endplate thickness	p<0.05	p<0.05
	Depth implant positioning	p<0.05	p<0.05
	Interaction	p<0.05	0,73
AL upper	Endplate thickness	p<0.05	0,23
	Depth implant positioning	p<0.05	p<0.05
	Interaction	p<0.05	0,15
AL middle	Endplate thickness	0,85	p<0.05
	Depth implant positioning	p<0.05	p<0.05
	Interaction	0,49	p<0.05
AL lower	Endplate thickness	0,15	p<0.05
	Depth implant positioning	p<0.05	p<0.05
	Interaction	0,43	0,90
PL upper	Endplate thickness	0,14	p<0.05
	Depth implant positioning	p<0.05	p<0.05
	Interaction	0,98	p<0.05
PL middle	Endplate thickness	0,07	p<0.05
	Depth implant positioning	0,35	p<0.05
	Interaction	p<0.05	p<0.05
PL lower	Endplate thickness	0,46	p<0.05
	Depth implant positioning	0,27	p<0.05
	Interaction	0,92	p<0.05
P upper	Endplate thickness	p<0.05	p<0.05
	Depth implant positioning	p<0.05	p<0.05
	Interaction	p<0.05	p<0.05

Table 4 - P-values from T-tests, performed to test the difference of mean of cortex strains between the different combinations of depth endplate thickness/depth implant positioning and the intact spine segment.

Endplate thickness		0.5mm		0.25mm		0mm	
Principal Strain		ε1 (maximum)	ε2 (minimum)	ε1 (maximum)	ε2 (minimum)	ε1 (maximum)	ε2 (minimum)
Strain gauge	Depth implant position						
A upper	-	-	-	-	-	-	-
A middle	Anterior	0,45	p<0.05	p<0.05	p<0.05	p<0.05	p<0.05
	Centered	0,19	0,32	p<0.05	p<0.05	p<0.05	p<0.05
	Posterior	0,08	0,10	0.06	p<0.05	p<0.05	p<0.05
A lower	Anterior	p<0.05	0,06	p<0.05	0.20	p<0.05	0,43
	Centered	p<0.05	0,28	0.07	0.09	0,09	0.07
	Posterior	p<0.05	p<0.05	0.15	p<0.05	0,54	p<0.05
AL upper	Anterior	p<0.05	p<0.05	0,12	p<0.05	0,695	p<0.05
	Centered	p<0.05	0,10	p<0.05	0,12	p<0.05	0,06
	Posterior	0,14	p<0.05	p<0.05	0,17	p<0.05	0,10
AL middle	Anterior	p<0.05	p<0.05	0,09	p<0.05	p<0.05	p<0.05
	Centered	0,15	0,32	0,11	p<0.05	0,18	p<0.05
	Posterior	0,06	p<0.05	0,12	p<0.05	0,37	p<0.05
AL lower	Anterior	p<0.05	p<0.05	p<0.05	p<0.05	p<0.05	p<0.05
	Centered	0,09	p<0.05	0.07	p<0.05	0,11	0.07
	Posterior	0,07	0,10	0,14	0,07	0,95	p<0.05
PL upper	Anterior	p<0.05	p<0.05	0,12	p<0.05	0,09	p<0.05
	Centered	0,10	0.14	0,14	p<0.05	0,21	p<0.05
	Posterior	p<0.05	p<0.05	p<0.05	p<0.05	p<0.05	p<0.05
PL middle	Anterior	0,09	p<0.05	0.08	p<0.05	0,45	p<0.05
	Centered	0,17	0,15	0,16	p<0.05	0,22	p<0.05
	Posterior	0,57	p<0.05	0,17	p<0.05	0,32	p<0.05
PL lower	Anterior	0,33	0,37	0,23	0,24	0,32	0,17
	Centered	0,18	p<0.05	0,21	p<0.05	0,24	p<0.05
	Posterior	0,53	0,58	0,15	p<0.05	0,42	p<0.05
P upper	Anterior	p<0.05	p<0.05	p<0.05	p<0.05	p<0.05	0,11
	Centered	p<0.05	p<0.05	p<0.05	p<0.05	p<0.05	p<0.05
	Posterior	p<0.05	p<0.05	p<0.05	p<0.05	p<0.05	p<0.05